Robust Matching of 3D Lung Vessel Trees

Dirk Smeets*, Pieter Bruyninckx, Johannes Keustermans,
Dirk Vandermeulen, and Paul Suetens

K.U.Leuven, Faculty of Engineering, ESAT/PSI
Medical Imaging Research Center, UZ Gasthuisberg,
Herestraat 49 bus 7003, B-3000 Leuven, Belgium

Abstract. In order to study ventilation or to extract other functional information of the lungs, intra-patient matching of scans at a different inspiration level is valuable as an examination tool. In this paper, a method for robust 3D tree matching is proposed as an independent registration method or as a guide for other, e.g. voxel-based, types of registration. For the first time, the 3D tree is represented by intrinsic matrices, reference frame independent descriptions containing the geodesic or Euclidean distance between each pair of detected bifurcations. Marginalization of point pair probabilities based on the intrinsic matrices provides soft assign correspondences between the two trees. This global correspondence model is combined with local bifurcation similarity models, based on the shape of the adjoining vessels and the local gray value distribution. As a proof of concept of this general matching approach, the method is applied for matching lung vessel trees acquired from CT images in the inhale and exhale phase of the respiratory cycle.

1 Introduction

The pulmonary ventilation, i.e. the inflow and outflow of air between the lungs and atmosphere, is the result of the movement of the diaphragm or the ribs leading to small pressure differences between the alveoli and the atmosphere. Quantification of pulmonary ventilation is a clinically important functional component in lung diagnosis. Pulmonary ventilation can be studied using several CT images in one breathing cycle (4D CT) [1]. In radiotherapy treatment, extraction of the lung deformation is important for correction of tumor motion, leading to a more accurate irradiation.

Matching, i.e. spatially aligning images (also referred as registration), inspiration and expiration scans is a challenging task because of the substantial, locally varying deformations during respiration [2]. To capture these deformations, a non-rigid registration is required, which can be image-based, surface-based and/or landmark-based. Generally, a non-rigid registration algorithm requires three components: a similarity measure, a transformation model and an optimization process.

* Corresponding author: dirk.smeets@uz.kuleuven.be

In image registration, common voxel similarity measures are sum of square differences (SSD), correlation coefficient (CC) and mutual information (MI) [3, 4]. To regularize the transformation, popular transformation models are elastic models, viscous fluid models, spline-based techniques, finite element models or optical flow techniques [3]. Voxel-similarity based techniques have been applied to lung matching in [5–7]. They have the advantage that dense and generally accurate correspondences are obtained. Disadvantages are the sensitivity to the initialization and the computational demands. Surface-based registration methods use a similarity measure that is a function of the distances between points on the two surfaces. Thin-plate splines are popular for regularization of the transformation. A combination of an voxel-similarity based and surface based registration for lung matching is presented in [8]. Generally, landmark-based non-rigid registration algorithms allow large deformations. Because of their sparsity, they are very efficient. In [9] bifurcations of lung vessels are first detected after which these landmarks are matched by comparing the 3D local shape context of each pair of bifurcations with the χ^2-distance.

In this paper, we present a robust registration method for matching vessel trees. After detecting candidate bifurcations (Sec. 2.1), correspondences are established by combining a global and a local bifurcation similarity model. For the novel global model (Sec. 2.3), the tree is represented by two reference frame independent, hence intrinsic, matrices: the Euclidean (rigid transformation invariant) and geodesic (isometric deformation invariant) distance matrix. Marginalization of point pair probabilities provides soft (not binary) correspondences between the detected bifurcations of the two trees. The local bifurcation similarity model reflects correspondences based on local intensities and is explained in Sec. 2.3. The optimization to obtain hard correspondences is done using a spectral decomposition technique (Sec. 2.4). The proof of concept of the general matching approach is shown in Sec. 3. Finally we draw some conclusions.

2 Method

The goal of the proposed matching framework is to establish correspondences between characteristic points in the image, independent of the reference frame (translation and rotation invariant) and, for characteristic points in structures that are assumed to deform isometrically, invariant for isometric deformations. Isometries are defined as distance-preserving isomorphisms between metric spaces, which generally means that structures only bend without stretching. The bifurcations, the splittings of the vessels in two or more parts, are chosen as characteristic points, although their detection is not the main goal of this paper. We then assume the vessel tree to deform isometrically. This assumption of nearly constant vessel length has been made before in a.o. [10] and [11].

2.1 Bifurcation detection

Bifurcations are locations where a blood vessel splits into two smaller vessels. A subset of the bifurcations that involves only major vessels can be detected in a robust way by analyzing the skeletonization of the segmented vessels.

As preprocessing, the lungs are segmented by keeping the largest connected component of all voxels with an intensity lower than -200 HU. A morphological closing operator includes the lung vessels to the segmentation and a subsequent erosion operation removes the ribs from the segmentation. Then, a rough segmentation of the major blood vessels within the lung is obtained by thresholding at -200 HU. Cavities in binary segmentation smaller than 10 voxels are closed. The skeletonization of the segmentation localizes the major bifurcations and is obtained through a 3D distance transformation by homotopic thinning [12]. Since bifurcations are locations where three vessels join, they are characterized as skeleton voxels having three different neighbors belonging to the skeleton. Afterwards, bifurcations are discarded that have a probability lower than $0.5/\sqrt{2\pi\sigma^2}$ according to a statistical intensity model. The vessel intensities I_k are assumed to be Gaussian distributed

$$P(c_{vessel}|I_k) = \frac{1}{\sqrt{2\pi\sigma^2}} \exp\left(-\frac{(I_k-\mu)^2}{\sigma^2}\right), \tag{1}$$

with experimentally determined parameters ($\mu = -40$ HU and $\sigma = 65$ HU).

2.2 Global correspondence model

After the vessel bifurcations are detected, soft correspondences are established based on a global and a local correspondence model, both independent of rigid and isometric deformations of the considered vessel trees.

Intrinsic vessel tree representation. Each tree is intrinsically represented by a Euclidean distance matrix $E = [d_{\mathbb{R}^3,ij}]$ (EDM), containing Euclidean distances between each pair of bifurcations, and a geodesic distance matrix $G = [g_{ij}]$ (GDM). Each element g_{ij} corresponds to the geodesic distance between the bifurcations i and j. This distance is the distance between i and j along the vessels and is computed with the fast marching method in an image containing a soft segmented vessel tree using Eq. (1). Isometric vessel deformations, by definition, leave these geodesic distances unchanged. Therefore, the GDM is invariant to the bending of the vessels. On the other hand, the EDM is only invariant to rigid transformations (and, when normalized, invariant to scale variations) of the vessel tree. However, Euclidean distance computation is expected to be more robust against noise than geodesic distance computation since the error accumulates along the geodesic, i.e. the shortest path. Both the EDM and the GDM are symmetric and uniquely defined up to an arbitrary simultaneous permutation of their rows and columns due to the arbitrary sampling order of the bifurcations. An example of a lung vessel tree, represented by a GDM and a EDM, is shown in Fig. 1.

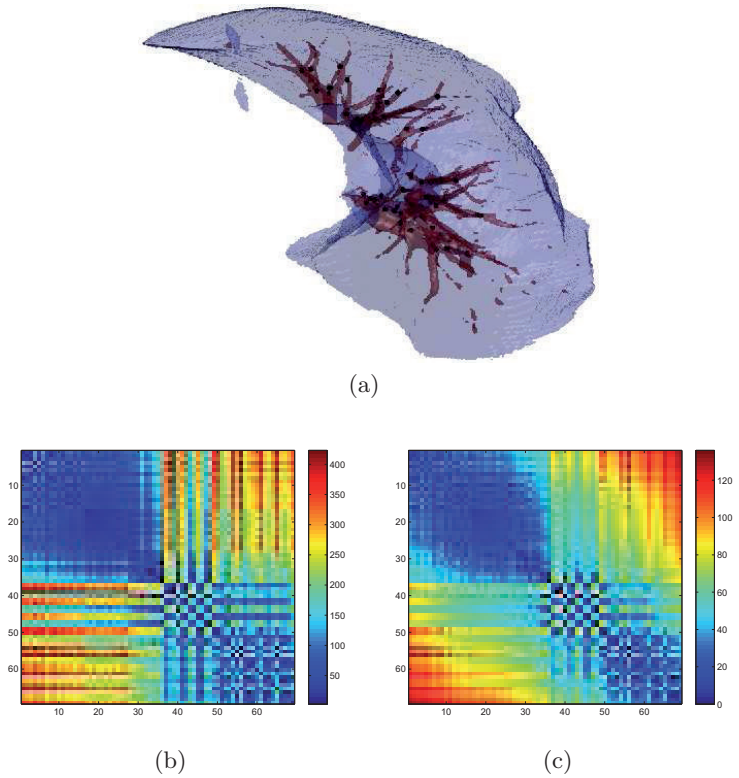

(a) (b) (c)

Fig. 1. A lung vessel tree with detected bifurcations (a) is represented by a geodesic (b) and a Euclidean (c) distance matrix, containing the geodesic or Euclidean distance between each pair of bifurcations.

Soft correspondences of the global model. A probabilistic framework is used to estimate the probability that a bifurcation i of one tree corresponds with a bifurcations k of the other tree. It is applied twice, once for the EDM and once for the GDM. We will explain the framework using the GDM.

Given two lung vessel trees, represented by GDMs, the probability that the pair of bifurcations (i, j) of the first tree G_1 correponds with the pair (k, l) of the second tree G_2 is assumed to be normally distributed,

$$P(C_{(i,j),(k,l)}) = \frac{1}{\sqrt{2\pi\sigma^2}} \exp\left(-\frac{(g_{1,ij} - g_{2,kl})^2}{\sigma^2}\right), \tag{2}$$

with σ chosen to be 1 and $g_{1,ij}$ an element of the GDM representing the first tree. It reflects the assumption that geodesic distances between pairs of bifurcations are preserved, obeying an isometric deformation. The probability that a

bifurcation i corresponds with k is then given by

$$P(C_{i,k}) = \sum_j \sum_l P(C_{(i,j),(k,l)}) = m_{G,ik}, \tag{3}$$

from which the soft correspondence matrix, $M_G = [m_{G,ik}]$, is constructed.

The same procedure is followed to obtain an assignment matrix M_E based on the EDM as intrinsic tree representation. This matrix is expected to be more robust against noise, but varies under isometric deformations of the vessel tree, contrary to M_G.

2.3 Local correspondence model

Complementary to the global bifurcation similarity model, a local model based on intensities is implemented. In the computer vision literature a large number of local image descriptors are proposed, see for example [13].

In this paper, the n-SIFT (scale invariant feature transform) image descriptor is used [14], which summarizes a cubic voxel region centered at the feature location, in casu the bifurcation location. The cube is divided into 64 subregions, each using a 60 bin histogram to summarize the gradients of the voxels in the subregion. This results in a 3840-dimensional feature vector $\mathbf{f}$ by combining the histograms in a vector after weighting by a Gaussian centered at the feature location. The probability that a bifurcation i corresponds with k is then proportional to

$$P(C_{i,k}) \propto \exp(- \parallel \mathbf{f}_i - \mathbf{f}_k \parallel^2) = m_{L,ik}, \tag{4}$$

2.4 Spectral matching

The combined match matrix M_C is found as the pointwise product of the match matrices of the separate models, $m_{C,ik} = m_{G,ik}.m_{E,ik}.m_{L,ik}$ (i.e. product of the corresponding probabilities). To establish hard correspondences (one-to-one mapping), the algorithm proposed by Scott and Longuet-Higgins [15] is used. It applies a singular value decomposition to M_C ($M_C = U\Sigma V^T$) and computes the orthogonal matrix $M'_C = U\tilde{I}_n V^T$, with $\tilde{I}_n$ a pseudo-identity matrix. Two bifurcations i and k match if $m'_{C,ik}$ is both the greatest element in its row and the greatest in its column.

3 Experimental results

The described matching framework is evaluated using a publicly available 4D CT thorax dataset of the Léon Bérard Cancer Center & CREATIS lab (Lyon, France), called "POPI-model". It contains 10 3D volumes representing the different phases of the average breathing cycle, with an axial resolution of 0.976562 mm $\times$ 0.976562 mm and a slice thickness of 2 mm. Also, 3D landmarks, indicated by medical experts, and vector fields describing the motion of the lung, are available [16].

3.1 Matching manually indicated landmarks

First, the matching framework is evaluated using manually indicated landmarks to examine the performance independent of the bifurcation detection step. For this purpose, all 40 landmarks are used in one CT image (end-inhalation phase), while varying the number of landmarks in the other image. The result of this experiment, expressed as the percentage of correct correspondences in function of the percentage outliers of the total number of landmarks, is shown in Fig. 2 for different images in the respiratory cycle. Since not all landmarks are located in the vessels and therefore geodesic distances are not meaningful, M_G is not computed.

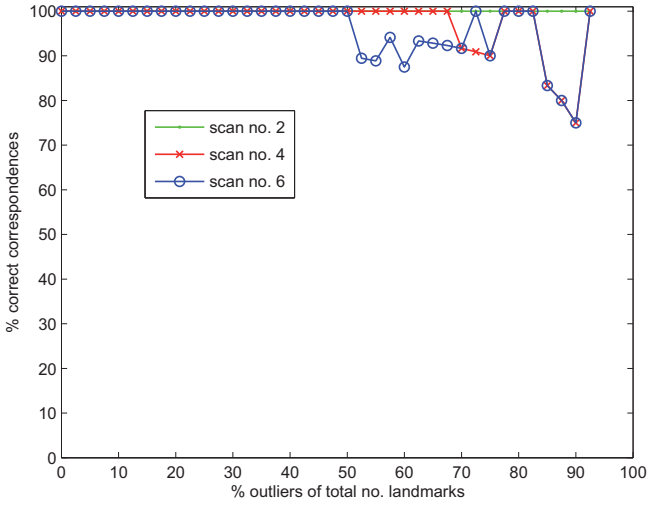

Fig. 2. Results of the framework for matching manually indicated landmarks expressed as the percentage of correct correspondences in function of the percentage outliers. The three curves correspond with different scans in the respiratory cycle, in which scan no. 1 is end-inhale and scan no. 6 end-exhale.

These results show that even for a large number of outliers good correspondences are still found. Consequently, it can be expected that not all bifurcations detected in one image must be present in the other image. Also, a small decrease in performance can be noticed when more lung deformation is present (end-exhale vs. end-inhale), probably because the Euclidean distance matrix (used in the global correspondence model) is not invariant for these deformations.

Second, the robustness against landmark positioning errors is examined. Therefore, we add uniform distributed noise in each direction to one set of landmarks and vary the maximum amplitude of the noise. Fig. 3 shows the percentage of correct correspondences in function of this maximum amplitude,

averaged over 15 runs per noise level. These results show that indication errors of more than 5 mm (± 5 voxels in x and y direction and 2.5 voxels in z direction) decrease the matching performance. It is therefore expected that the localization of bifurcations during automatic bifurcation detection must not be extremely accurate in order to still obtain good correspondences.

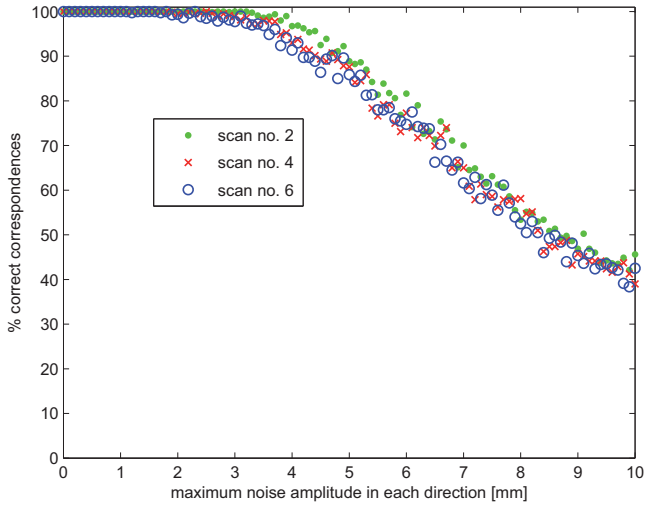

Fig. 3. Indication error dependence, expressed as the percentage of correct correspondences in function of the maximum amplitude of the added uniform noise. The three curves correspond with different scans in the respiratory cycle, in which scan no. 1 is end-inhale and scan no. 6 end-exhale.

3.2 Matching automatically detected bifurcations

Next, the framework is evaluated for the task of matching 3D vessel trees by means of automatically detected bifurcations. The result of matching the end-inhale with the end-exhale vessel tree is shown in Fig. 4, clarifying that most correspondence pairs are correct. It is also clear that simple thresholding has resulted in oversegmentation in one of the two images. This, however, did not affect the automatic matching.

The performance of matching automatically detected bifurcations is quantified using the dense deformation field that is available in the public dataset (POPI-model). This deformation field is obtained using a parametric image-based registration [17, 18, 16]. The average target registration error in the manual landmarks is 1.0 mm with a standard deviation of 0.5 mm.

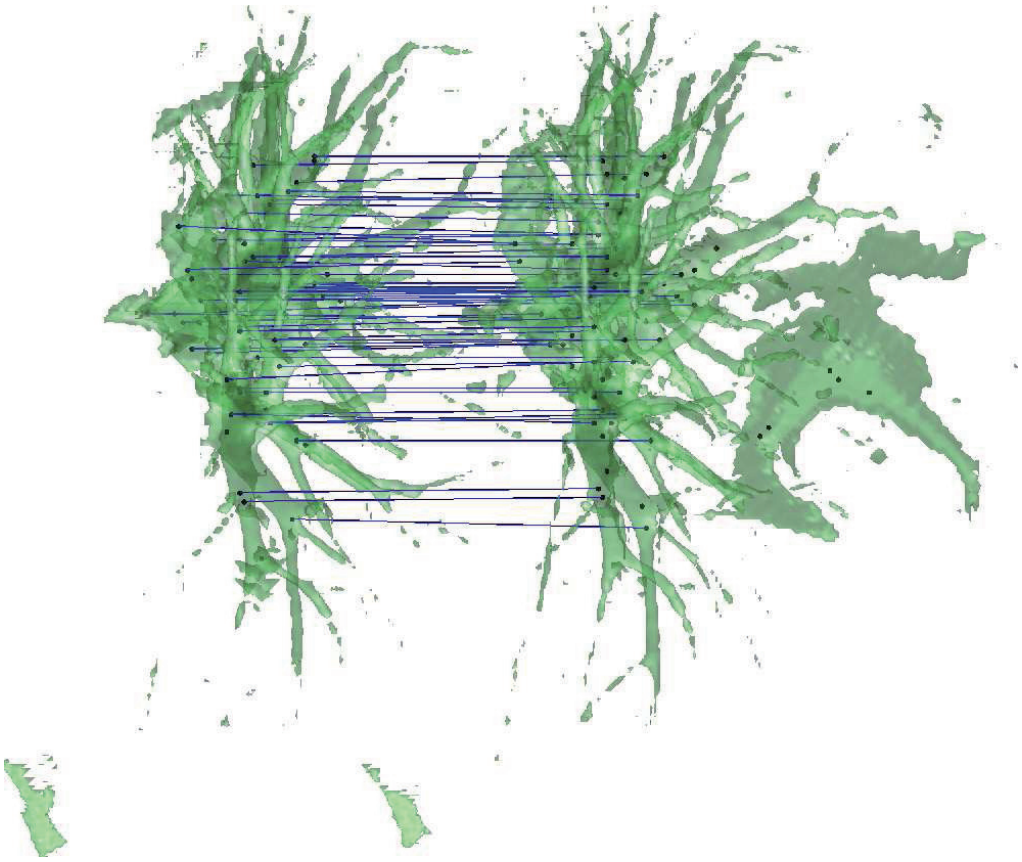

Fig. 4. Qualitative evaluation for matching 3D vessel trees by means of automatically detected bifurcations.

Fig. 5 illustrates the accuracy of the matching of the end-inhale scan with all other scans. It shows histograms of the registration error (in each direction and in absolute value) for all bifurcations. The average registration error is 2.31 mm, the median 1.84 mm and the maximum 24.0 mm. Only for 0.21% of the bifurcation matches the absolute registration error is larger than 1.5 cm, demonstrating the robustness of the matching algorithm.

4 Conclusion

A robust matching framework is proposed, combining two global and one local landmark similarity model. The results of matching manually indicated landmarks demonstrate the potential of the proposed method for matching landmarks in unimodal medical images independent of the translation and rotation between both images. A high number of outliers is allowed when the landmarks

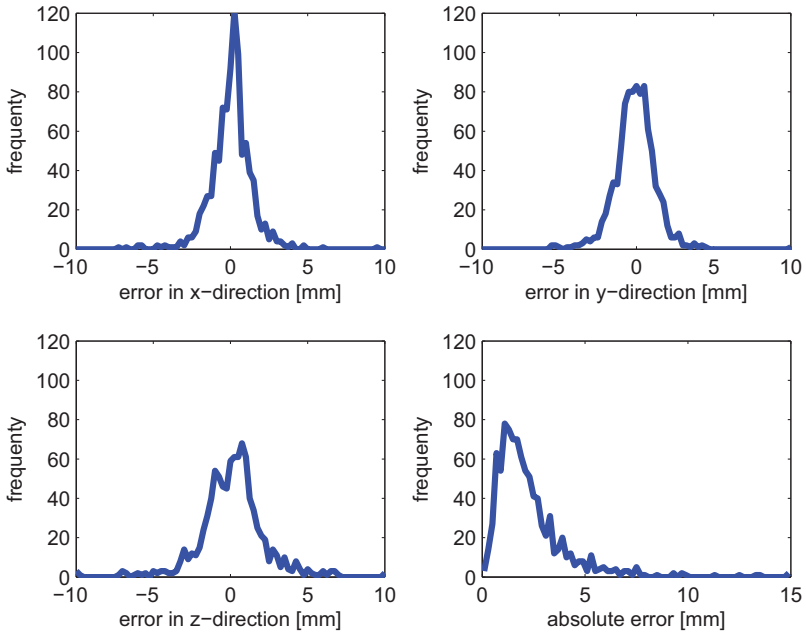

Fig. 5. Histograms of the registration error (in each direction and in absolute value) for all bifurcations give an impression of the matching accuracy.

in the image are well located. Moreover, we demonstrated that the matching framework can also be used for automatically detected landmarks, in this case lung bifurcations extracted from CT data.

As future work, we see some applications of the soft correspondences for robust initialization of an iterative non-rigid, e.g. voxel-based, registration method.

References

1. Guerrero, T., Sanders, K., Castillo, E., Zhang, Y., Bidaut, L., Pan, T., Komaki, R.: Dynamic ventilation imaging from four-dimensional computed tomography. Phys. Med. Biol. **51** (2006) 777–791
2. Sluimer, I., Schilham, A., Prokop, M., van Ginneken, B.: Computer analysis of computed tomography scans of the lung: a survey. IEEE Trans. Med. Imaging **25**(4) (2006) 385–405
3. Crum, W.R., Hartkens, T., Hill, D.L.G.: Non-rigid image registration: theory and practice. Br J Radiol **77 Spec No 2** (2004) S140–53
4. Pluim, J.P.W., Maintz, J.B.A., Viergever, M.A.: Mutual information based registration of medical images: A survey. IEEE Trans. Med. Imaging **22**(8) (2003) 986–1004

5. Dougherty, L., Asmuth, J.C., Gefter, W.B.: Alignment of ct lung volumes with an optical flow method. Academic Radiology **10**(3) (2003) 249 – 254
6. Stancanello, J., Berna, E., Cavedon, C., Francescon, P., Loeckx, D., Cerveri, P., Ferrigno, G., Baselli, G.: Preliminary study on the use of nonrigid registration for thoraco-abdominal radiosurgery. Med Phys. **32**(12) (2005) 3777–85
7. Loeckx, D.: Automated Nonrigid Intra-Patient Image Registration Using B-Splines. PhD thesis, K.U.Leuven (2006)
8. Kaus, M., Netsch, T., Kabus, S., Pekar, V., McNutt, T., Fischer, B.: Estimation of organ motion from 4D CT for 4D radiation therapy planning of lung cancer. In: MICCAI. Volume 3217 of LNCS. (2004) 1017–1024
9. Hilsmann, A., Vik, T., Kaus, M., Franks, K., Bissonette, J.P., Purdie, T., Beziak, A., Aach, T.: Deformable 4DCT lung registration with vessel bifurcations. In: CARS. (2007)
10. Klabunde, R.E.: Determinants of resistance to flow. http://www.cvphysiology.com/Hemodynamics/H003.htm (august 2008)
11. Groher, M., Zikic, D., Navab, N.: Deformable 2D-3D registration of vascular structures in a one view scenario. IEEE Trans Med Imaging **28**(6) (2009) 847–60
12. Selle, D.: Analyse von gefässstrukturen in medizinischen schichtdatensätzen für die computergestützte operationsplanung. PhD thesis, Aachen (2000)
13. Mikolajczyk, K., Schmid, C.: A performance evaluation of local descriptors. IEEE Trans. Pattern Anal. Mach. Intell. **27**(10) (2005) 1615–1630
14. Cheung, W., Hamarneh, G.: n-sift: n-dimensional scale invariant feature transform. Trans. Img. Proc. **18**(9) (2009) 2012–2021
15. Scott, G.L., Longuet-Higgins, H.C.: An algorithm for associating the features of two images. Proc. R. Soc. Lond. B **244** (1991) 21–26
16. Vandemeulebroucke, J., Sarrut, D., Clarysse, P.: The POPI-model, a point-validated pixel-based breathing thorax model. In: Conference on the Use of Computers in Radiation Therapy. (2007)
17. Rueckert, D., Sonoda, L.I., Hayes, C., Hill, D.L.G., Leach, M.O., Hawkes, D.J.: Nonrigid registration using free-form deformations: Application to breast mr images. IEEE Transactions on Medical Imaging **18** (1999) 712–721
18. Delhay, B., Clarysse, P., Magnin, I.E.: Locally adapted spatio-temporal deformation model for dense motion estimation in periodic cardiac image sequences. In: FIMH'07: Proceedings of the 4th international conference on Functional imaging and modeling of the heart, Berlin, Heidelberg, Springer-Verlag (2007) 393–402